Improved Measurement of Asteroid (4) Vesta's Rotational Axis Orientation

Jian-Yang Li[a,*], Peter C. Thomas[b], Brian Carcich[b], Max J. Mutchler[c], Lucy A. McFadden[d], Christopher T. Russell[e], Stacy S. Weinstein-Weiss[f], Marc D. Rayman[f], Carol A. Raymond[f]

[a] Department of Astronomy, University of Maryland, College Park, MD 20742

[b] Center for Radiophysics and Space Research, Cornell University, Ithaca, NY 14853

[c] Space Telescope Science Institute, Baltimore, MD 21218

[d] NASA Goddard Space Flight Center, Greenbelt, MD 20771

[e] IGPP & ESS, University of California at Los Angeles, CA 90095

[f] Jet Propulsion Laboratory, California Institute of Technology, Pasadena, CA 91109

New manuscript submitted to Icarus

Manuscript pages: 32

Number of tables: 5

Number of figures: 5

Submitted on August 1, 2010

Abstract

We report an improved measurement of the rotational axis orientation of Asteroid (4) Vesta. By analyzing and combining all previous measurements using limb-fitting technique from ground/HST data collected from 1983 to 2006, we derive a pole solution of (RA=307.2º, Dec=43.4º). Images of Vesta acquired with the Wide Field Camera 3 onboard Hubble Space Telescope (HST) in February 2010 are combined with images from the Wide Field Planetary Camera 2 on HST obtained in 1994, 1996, and 2007 at similar spatial resolution and wavelengths to perform new measurements. Control point stereogrammetry returns a pole solution of (305.1º, 43.4º). An alternate method tracks surface features and fits their projected paths with ellipses to determine a great circle containing the pole for each HST observation. Combined, the four great circles yield a pole solution of (309.4º, 41.9º). These three solutions obtained with almost independent methods are within 3.5º of each other, suggesting a robust solution. Combining the results from all three techniques, we propose an improved value of the rotational axis of Vesta as RA=307.5º±3.1º, Dec=43.1º±1.2º (1-σ error). This new solution differs from the currently adopted pole (301º, 41º) reported by Thomas et al. (1997a) [Icarus 128, 88-94] by 5.3º. It changes the obliquity of Vesta by only ~1º, but increases the Sun-centered RA of Vesta at equinox by ~10º, and postpones the date of equinox by ~50 days. The change of the pole position is less than the resolution of all previous images of Vesta, and should not change the main science conclusions of previous research about Vesta.

Keywords: Asteroid Vesta; Asteroids, rotation; Asteroids, surfaces

1. Introduction

As a surviving protoplanet with an intact basaltic crust and differentiated interior, Asteroid (4) Vesta provides us with unique information for understanding the formation process and early evolution of terrestrial planets. Spin pole orientation of an asteroid is one of its fundamental properties, determining its obliquity and seasons, and therefore the surface thermal environment on the object.

Vesta's pole orientation has been previously measured from ground-based, spatially resolved images using speckle interferometry (SI) (Drummond and Hege, 1989) and adaptive optics (AO) (e.g., Drummond et al., 2008), as well as from Hubble Space Telescope (HST) images. The currently adopted pole orientation of Vesta is (RA=301°, Dec=41°) (Thomas et al., 1997a) based on HST Wide Field Planetary Camera 2 (WFPC2) images collected in 1994 and 1996 (Fig. 1). Table 1 lists all other measurements of Vesta's pole orientation mainly derived from ground-based images. Due to the limitation of spatial resolution and the small angular size of Vesta, these previous determinations have uncertainties typically 5°-10° in the sky and range from 274° to 335° in RA and from 8° to 48° in Dec (Table 1).

There are primarily two methods used to derive the pole orientation of Vesta from spatially resolved images: control point stereogrammetry and limb fitting.

Control point stereogrammetry concurrently calculates surface features latitudes, longitudes, and radii, as well as the spin pole orientation. The total squared difference between the measurements and the predicted positions of control points were minimized iteratively by adjusting the solutions to the coordinates of control points and the pole orientation. Limb fitting

is a widely adopted technique to determine an object's 3-D shape (e.g., Thomas et al. 1997b; Drummond et al., 2008). If an object's rotation has relaxed to its largest moment of inertia, then its rotational axis is aligned with the shortest axis. All measurements listed in Table 1 are derived with limb-fitting. The accuracy of both methods is mostly limited by the small angular size of Vesta that can only be resolved to less than 15 pixels in diameter in all cases. Generally, the precision of the limb-finding software used in Thomas et al. (1997a) is ~0.1 pixels. For small disks such as these, the accuracy of the determination may be reduced by the photometric effects of having part of the disk within a few pixels of the limb. If the phase angle is not zero, then the terminator will depart from the Vesta's dark limb, requiring some corrections. But comparisons to occultation data indicated accuracies under 10 km or ~0.2 pixels for Vesta.

NASA's Dawn spacecraft, launched in September 2007, is on its way to rendezvous with Vesta starting from July 2011 and Asteroid (1) Ceres in February 2015. The spacecraft will use its three scientific instruments to characterize each body from orbit (Russell et al., 2007; Rayman et al., 2006). The pole orientation of Vesta determines the illumination conditions on the asteroid during Dawn's stay, and is an important factor for designing the spacecraft trajectory around Vesta. A better pole orientation measurement of Vesta would significantly benefit the overall science plan and the navigation plan of Dawn mission.

In this paper, we report an improved determination of Vesta's rotational axis orientation derived from a detailed analysis of all previously reported results and new measurements from combined newly acquired and previous HST data.

2. Analysis

2.1 Combined limb-fitting solutions

First we considered the previous pole solutions from ground/HST observations derived using limb-fitting methods (Table 1). The combination is not a simple (weighted) average of all solutions in RA and Dec. Instead, we extracted only the most reliable information from those solutions, and combined them with a statistical analysis.

The uncertainty of the pole solutions from limb-fitting depends critically on the measurement of the change of the long and short axes of the projected disk, and therefore could be very sensitive to the uncertainty of fitted shape model. For example, the solution from February 11, 2006 observation has an extremely large uncertainty on the *c*-axis fitted shape (Drummond and Christou, 2008), resulting in a pole solution with Dec=8º, which is highly unlikely. Drummond et al. (1998) noticed that the large scatter between the solutions from different observations is probably due to the uncertainties in the fitted shape models. On the other hand, the projected direction of the pole in the sky plane does not directly depend on the actual shape and shape uncertainties. For sub-Earth latitudes of less than 30º for Vesta, the uncertainty of the projected pole position-angle would only slightly depend on sub-observer latitude. Therefore, we decided to only use the projected direction of the pole measured from all previous data, and take advantage of the large scatter of Vesta in RA over the 13 observations (Fig. 2).

For each reported pole solution, we used the observing date to derive the great circle on the celestial sphere containing that pole solution, and then took a maximum likelihood approach (Bevington and Robinson, 1992) to combine all the great circles in a summary pole solution. We

assumed that, for a measured great circle, i, the probability that the true pole is at distance d from the great circle is a Gaussian, $P_i(d) = A_i \exp(-\frac{d^2}{2\sigma_i^2})$, where A_i is a normalization factor, and σ_i is the standard deviation for this great circle. The probability density function (PDF) of the true pole at RA=α and Dec=δ, $P(\alpha, \delta)$, is the multiplications of all P_i's because all individual measurements are independent. The combined solution is where $P(\alpha, \delta)$ has the maximum value. The error ellipses can be derived from a fit to $P(\alpha, \delta)$ with a 2-D Gaussian. This approach is fundamentally a standard weighted least square method to derive the best value from multiple measurements of a physical quantity.

We used the reported uncertainty of each pole solution as the σ_i to start with in the above approach. However, those error bars are statistical error bars derived from fitting each observation with a triaxial ellipsoidal shape model, not necessarily representing the standard deviation of the PDFs. Indeed, the reduced $\chi^2 \equiv \frac{1}{N-2}\sum_i \frac{d_i^2}{\sigma_i^2}$, where d_i is the distance of the combined pole solution to great circle i, and the summation is over all N=13 great circles, is about 2.2 rather than unity. This suggests that the σ_i's we used were very likely underestimated. In the SI and AO data, the shape of the projected disk of Vesta was affected by phase angle, sub-solar latitude, and sub-Earth latitude. The telescope optics could also introduce some artifacts into the images. These factors could all bring in systematic uncertainty for each individual solution listed in Table 1, while the reported uncertainties do not account for these systematic uncertainties.

On the other hand, note that the 13 observations Vesta are almost evenly located over ecliptic longitude; their sub-Earth latitudes cover the whole range from -20° to +20° (Fig. 2); and

their phase angles also randomly scatter (Table 1). Since the systematic error of individual pole measurement from limb-fitting is more likely dominated by observing geometry than instruments, when we combine all 13 observations, their individual systematic error would become random and behave like statistical error. If we further assume that the uncertainty introduced by geometry can be described by a normal distribution with a standard deviation σ_s, then we can quadratically add it to all the reported error bars in the above approach. A value of 3.1° for σ_s was adopted in order to make the reduced χ^2 unity. This 3.1° is not necessarily the true "systematic error", but just the best numerical value we had to use to make our model statistically self-consistent. In practice, it did reduce the weights of some solutions with extremely small errors of less than 1°. Also note that the 10° error for HST measurement listed in Table 1 actually includes an estimate of systematic uncertainty of limb-fitting from a single observation (Thomas et al., 1997a); we therefore assumed a numerical error of 2° here for HST data in our analysis.

The maximum likelihood approach yielded a solution of (307.2°, 43.4°), as shown in Fig. 3. The 1-σ errors of the solution are 3.4° and 1.3° in RA and Dec, respectively. It is worth noting that the great circle from the unlikely solution of February 11, 2006 data does not appear to be peculiar compared to all other great circles, and excluding it only changes the final result by 0.5° and increases the error in RA by 0.1°. The great circles are actually immune from any uncertainties in the fitted *c*-axis. This demonstrates that the strategy we took effectively filtered out most unreliable information contained in each individual solution.

2.2 Control point stereogrammetry

Since Thomas et al. (1997a) applied the control point stereogrammetry method to measure Vesta's pole from HST images collected in 1994 and 1996, Li et al. (2010) have acquired new HST images in 2007 to map the southern hemisphere of Vesta. In addition, we obtained more images of Vesta in February 2010 specifically for the determination of Vesta's pole orientation. The new data were taken with the Wide Field Camera 3 (WFC3) newly installed on HST and operating at similar wavelengths. The HST images of Vesta are summarized in Table 2. The 1994, 1996, and 2007 data have a pixel scale of 0.046"/pixel, and the 2010 data 0.039"/pixel. The 1994 data and 2010 data have similar observer latitudes near 25º N according to current Vesta pole solutions. The 1996 data are nearly equator-on. The 2007 data have an observer latitude of ~20º S. The wide range of observer latitudes and the different celestial longitudes of the four data sets and the large number of relatively high signal-to-noise images from the 2010 HST observation should enable us to reach a more accurate measurement. We therefore applied control point stereogrammetry, and experimented with a new method, feature tracking, with all HST images to determine the pole orientation of Vesta. We discuss the results from control point in this section, and from feature tracking in the next section.

The software to implement the control point method was originally designed to process images all from a single detector (i.e., it uses only one camera model). In order to combine the 2010 data, which was collected by a different camera from that used in the previous data, we scaled the Earth range of the 2010 data so that the images can be treated as if they all have the same pixel instantaneous field of view of the WFPC2 CCD. The change of light time correction

introduced by this adjustment is about 90 seconds and the effect should be negligible in the 5.342-hr rotation of Vesta (Drummond et al., 1998). This should not affect the results.

From all 446 images, 17 control points were identified from 82 images, and only 12 control points dominate the final solution. The distribution of the 82 images used over four data sets and over filters is summarized in Table 3. The images were all in original contrast without any processing or enhancement from removing limb-darkening, although actual point identification relied on manual stretching of images.

The result from this method is (305.1°, 43.4°) (Fig. 1, open circle), with a minimized root mean square error of 0.16 pixels. While the formal statistical error is much smaller than the previous one for 1994 and 1996 data, the systematic error could be large. An uncertainty of 5° (1-σ) is a good estimate of the overall uncertainty in this solution.

From Table 3, more than 63% of the images used in this measurement were from the 2010 data, clearly due to the large number of available images from this observation and their relatively high signal-to-noise. The 2010 data therefore dominate the result. The next most dominant data is 2007 data (20% of the images). With a slightly smaller pixel scale, the 2007 data have the observer latitude on the opposite hemisphere of the 2010 data. The combination of all data therefore helped decrease any systematic error that is correlated with observer latitude, although the result should still be dominated by the 2010 data. Note that the currently used pole solution was derived from 1994 and 1996 data, the combination of which have observer latitudes biased more towards the northern hemisphere than does the combination of 2007 and 2010 datasets. Fig. 1 summarizes the various control point and limb findings. The new control point results are nearly midway between the individual 1994 and 1996 control point solutions. The

previous joint solution was affected by smaller residuals in the 1994 limbs and 1996 control point portions of the solutions. A separate control point solution done in 2008 only on the HST 2007 data gave a pole of (304º, 42º) (Thomas, priv. comm.), consistent with our solution derived above.

2.3 Feature tracking

The idea behind feature tracking is that, when an object rotates, the projected path of any surface feature across the disk is an ellipse. The long-axis of the projected elliptical path defines the normal to a great circle containing the object's pole; the axial ratio of the path is proportional to the sine of observer latitude. This method does not depend on the shape of the object.

We identified surface (bright and dark) features manually, and determined their centers by eye. In order to enhance the contrast of surface features, we experimented with removing the limb-darkening following the procedure to generate albedo maps (e.g., Li et al., 2010). We calculated a model disk from the best-fit, global average Minnaert photometric model (Minnaert, 1941), and either subtracted it from, or divided it into, the corresponding actual image. While ideally this step enhances the contrast but does not disturb the position of contrast features, in reality the removal of an underlying brightness gradient apparently can slightly change the positions of albedo features. Therefore the measurements from processed images have to be validated with the measurements from the original images. We applied the feature-tracking method to all four data sets on the original images as well as the contrast-enhanced images from both subtraction and division with the limb-darkening model. For 1994, 1996, and 2007 data, we used the F439W and F673N images, and for 2010 data we used the F373N and F469N images because of the relatively high contrast in short wavelength.

The position angle of the projected elliptical path of each feature was fit independently. Since only the data points for less than half of an ellipse are available, we have to impose some constraints on the parameters to be fitted; otherwise the fit often does not converge. Because the true pole orientation should be within 15° of the currently used solution, we started from the current shape model and pole solution to calculate the expected values of the fitted parameters, including the long and short axes, position angle, and pixel positions of the center. Then we set ±25% from the expected values as the possible ranges for the axes and center, and ±20° for position angles of the ellipse. We also noted that the center and the position angle of the ellipse are not all independent from each other, and thus tied them together in the fitting. If the fitted ellipse has any of its parameters on the edges of their respective searching ranges that we imposed, then that fit is discarded in the final results. Due to the limit of data, the size of the projected ellipse (therefore the sub-Earth latitude) is poorly constrained, but the position angle can be well constrained, with different fitting algorithms usually returning similar values for the orientation. The fitting routine returns numerical errors for all fitted parameters with the uncertainty of surface feature's pixel position assumed to be one pixel. The actual pixel position uncertainty should be smaller than one pixel, and thus the numerical errors returned by the fitting routine should be an overestimate. The fitted position angles of all ellipses from the same filter and the same data set are averaged and the error bars were propagated following standard statistical formalism to yield the final statistical error bar for the measurements from one observation through one particular filter.

The fitted position angles of Vesta's pole from 1996 and 2007 datasets from original images and two different enhancements agree with each other very well, and the results from two filters are in good agreement, too, within their respective statistical error bars. The typical

statistical error for each individual fit is ~2º. However, for 1994 data, the fit from images of two filters at original and different contrast enhancements scatter in a range of 12º, and the statistical error bar is ~5º. This is probably because of the relatively lower spatial resolution in 1994 data than other HST data. For the 2010 data, each individual fit has a typical statistical error of ~2º, similar to that of 1996 and 2007 data, suggesting that the statistical error is determined by spatial resolution and image quality. However, the fits to measurements from the original images and from different contrast enhancement returned results scattering in a large range from 10º to 37º, and sometimes the fits from the two filters and the same enhancement differ by up to 7º.

It is difficult to understand large scatter of the fits from the 2010 data. Possible causes include limb-darkening removal, systematic bias of the center positions of disks in all images when they are aligned, or systematic trend of the center positions of disks toward one direction. Contrast enhancement with both subtraction and division of limb-darkening model is based on the same set of original images, therefore disk center position should have the same effect over all three versions, and should not cause the discrepancy in fitted pole direction between them. The removal of limb-darkening can cause a shift of the apparent centers of albedo features, but in opposite directions for dark and bright features. However, the fitted orientations of ellipses from bright and from dark features do not differ much. With almost equal numbers of bright and dark features, any systematic bias caused by the contrast enhancement should cancel out.

Without understanding the cause of the large scatter, we consider that it is due to the systematic error introduced by limited spatial resolution and the technique itself, and combine them with some considerations. For the fits from two filters of the same data set and the same enhancement, they are independent. We combined the results and propagated the numerical

errors with the standard statistical method. For the fits from the same data set but different enhancement, due to the scatter especially for 1994 and 2010 data, we calculated the weighted average for each data set, and used the standard deviation to represent an estimate of systematic error. Then we add the standard deviation and the largest numerical error quadratically to represent the final error bar of the average for that data set. The projected angles of Vesta's orientation measured from four HST data sets are summarized in Table 4.

Finally, we combined the four great circles derived from the projected angles of Vesta's pole using the same approach we took in Section 2.1 to derive the pole solution of Vesta from the feature tracking method. The solution is (309.3º, 41.9º), as shown in Fig. 4 together with the error ellipse. Note that the error ellipse for this solution is probably conservative because the error estimate for each individual measurement from each data set is probably conservative.

2.4 Combined results

The three solutions we derived above are in good agreement with each other, all within a circle of 3.5º in diameter in the sky from 305º to 309º in RA and from 42º to 44º in Dec (Fig. 5). The limb-fitting method finds the pole from a shape model; the control point stereogrammetry solves the pole and part of the shape together; and feature-tracking is entirely independent of the shape of Vesta. The large scatter between the measurements from different observations using the same method indicates the possibly large systematic uncertainties for each individual measurement, primarily due to the limited spatial resolution of images. However, when the number of uncorrelated observations is large enough, systematic uncertainties in individual observations behave more like statistical uncertainties and tend to be averaged out when

combined. It is statistically significant that the combinations of a number of measurements with various methods converge to a small region.

The combination of all three solutions has two steps. Since the control-point method and feature-tracking method uses the same dataset and possibility some surface features in common, they are not entirely independent. We combine these two first following the maximum likelihood approach we took in Section 2.1, and then scale up the error ellipse to account for possible dependency between them. The scale factor should be between 1 and 2 for the entirely independent extreme and entirely dependent extreme, respectively. Then the control-point and feature-tracking combined solution is combined with the limb-fitting solution, which is entirely independent, using the same maximum likelihood method to derive the final combined solution and error ellipse. Following this two-step approach, we reached a solution of (307.7°±2.5°, 42.6°±1.0°) for a scale factor of 1, and (307.5°±3.1°, 43.1°±1.2°) for the conservative case of a scale factor of 2. They only differ by about 0.5°, well within the error bar. The combined solution is actually dominated by the limb-fitting result we derived in Section 2.1, and the scaling factor in the final combination has a small effect. We propose to use RA=307.5°, Dec=43.1° as the combined solution for Vesta's pole.

3. Discussion

The formal 1-σ uncertainty of the nominal solution is about 3.1° in RA and 1.2° in Dec. The actual ellipse on the sky corresponding to this uncertainty is 2.3°×1.2° due to the projection of spherical coordinate. We note that although this error bar is based on many assumptions of independency between different measurements and the reported error bars, we took several conservative backups in our derivation. Therefore the error estimate should be a fair estimate of

the combined pole solution. Of course the most conservative error ellipse would be the one that encompasses all error ellipses of all components to be combined shown in Fig. 5. Given the measurements from the three different methods all converge to a small region of 3.5º in diameter in the sky. The true pole should be within the nominal error bar we derived.

Compared to the currently adopted pole of (301º, 41º), the improved pole orientation represents a change of 5.3º. This is consistent with the uncertainty of the previous determination. The comparisons of the geometry parameters of Vesta based on the previous pole and our new measurement are listed in Table 5. The obliquity of Vesta from the new pole solution decreases from the value determined by the previous pole solution by ~1º, negligible if considering the error in the pole orientation. The newly determined pole orientation does not change the seasonal effect on Vesta. On the other hand, the new pole solution does increase the Sun-centered RA position of Vesta at its equinox by ~10º, and postpones the date by ~50 days.

The current Vesta-centered, longitude-latitude coordinate system is defined on the pole of (301º, 41º) and the accompanying prime meridian definition from Thomas et al. (1997a). Almost all the previous mapping efforts (Binzel et al., 1997; Li et al., 2010) as well as other studies such as Vesta's rotationally resolved spectroscopy (e.g., Reddy et al., 2010) and thermal properties (Chamberlain et al., 2007) have been based on these rotational elements. Still using Olbers to define the prime meridian on Vesta (Thomas et al., 1997a), we derived an argument of prime meridian of 284º for the new body-fixed coordinate system (Seidelmann et al., 2007) based on the improved pole solution. The 5.3º change in the solution of Vesta's pole orientation is below the resolution of all previous images of Vesta, therefore should not affect the main conclusions of all previous studies. We also note that the measurement of the pole orientation of Vesta will

soon be substantially revised to less than a tenth of a degree precision once Dawn approaches Vesta.

The largest impact of the improved measurement of Vesta's pole on Dawn mission is the change of illumination condition during Dawn's stay, in particular, the delay of the equinox date of Vesta by ~50 days. The currently used pole gives an equinox approximately on June 23, 2012, and the new solution yields an equinox around Aug 14, 2012. The decrease of the error ellipse from the previously measured pole will also help the trajectory design during approach and delivery of the spacecraft to Vesta orbit.

4. Summary

The currently adopted pole orientation of Vesta is based on HST observations in 1994 and 1996 (Thomas et al., 1997a). Many other measurements of Vesta's pole from the ground are reported. But all the results have 5º-10º errors and scatter in a large area in the sky. We performed a detailed analysis with all previously reported measurements of Vesta's pole, and acquired new Vesta images with HST to perform a combined measurement with previously collected HST images at similar spatial resolution and wavelength. The improved Vesta pole orientation determination will also benefit the Dawn mission, which will perform a detailed investigation of Vesta in July 2011 for a year.

We analyzed all previous measurements of Vesta's pole from ground/HST data with limb-fitting technique. We calculated the projected direction of Vesta's pole from each measurement, and combine the great circles determined from the projected pole. Statistical analysis yielded a solution of RA=307.2º±3.4º, Dec=43.4º±1.3º.

We applied control point stereogrammetry and feature tracking techniques on 1994, 1996, 2007, and the newly collected 2010 data from HST to measure the pole orientation of Vesta. Control point stereogrammetry simultaneously solved for the positions of 17 surface features from 82 images, and returned a result of RA=305.1º, Dec=43.4º, with an uncertainty of ~5º in RA and Dec.

Feature tracking tracked the apparent pixel positions of 9 surface features, and fitted their projected paths. The projected pole orientations in the sky plane for each set of data were derived from the orientation of elliptical paths, which determines great circles containing the pole. We enhanced the brightness contrast of images by removing a limb-darkening model from Vesta's disk in all images. The result from feature tracking method is RA=309.3º±6.8º, Dec=41.9º±1.5º.

Three solutions combined, we derived a pole orientation of Vesta at RA=307.5º±3.1º, Dec=43.1º±1.2º. The 3-σ region is 6.6º×3.6º in the sky along RA and Dec. The solutions from the three nearly independent methods are within 3.5º from each other, indicating a robust result.

Compared with the currently adopted pole at (301º, 41º) determined by Thomas et al. (1997a), the new solution changes by 5.3º, within the error bar of the previous pole solution. The change in the obliquity of Vesta is negligible (~1º), but the Sun-centered RA of Vesta at equinox increases by about ~10º, and the date of equinox is postponed by ~50 days. The main conclusions in previous studies on the topography and surface albedo mapping of Vesta should not be affected because the change of pole is smaller than the resolution of all previous images of Vesta.

Acknowledgement

Support for this work was provided by the National Aeronautics and Space Administration (NASA) through grant HST-GO-12049.01-A from the Space Telescope Science Institute, which is operated by the Association of Universities for Research in Astronomy, Inc., under NASA contract NAS5-26555. Part of this work was carried out at the Jet Propulsion Laboratory, California Institute of Technology, under a contrast with NASA. The authors are extremely grateful to Dr. Dennis Byrnes (Jet Propulsion Laboratory) and Dr. Tom Prettyman (Planetary Science Institute) for their reviews and inputs on the error analysis in our work. JYL would like to thank Dr. Xi Shao (University of Maryland) for the very helpful discussion on the statistical approach used in this work.

References

Bevington, P.R., Robinson, D.K., 1992. Data Reduction and Error Analysis for Physical Sciences, 2nd ed., McGraw-Hill, New York.

Binzel, R.P., Gaffey, M.J., Thomas, P.C., Zellner, B.H., Storrs, A.D., Wells, E.N., 1997. Geological mapping of Vesta from 1994 Hubble Space Telescope Images. Icarus 128, 95-103.

Chamberlain, M.A., Lovell, A.J., Sykes, M.V., 2007. Submillimeter lightcurves of Vesta. Icarus 192, 448-459.

Drummond, J.D., Eckart, A., Hege, E.K., 1988. Speckle interferometry of asteroids. IV. Reconstructed images of 4 Vesta. Icarus 73, 1-14.

Drummond, J.D., Hege, E.K., 1989. Speckle interferometry of asteroids. In: Binzel, P.B., Gehrels, T., Matthews, M.S. (Eds.), Asteroids II. Univ. of Arizona Press, Tucson, pp. 171-191.

Drummond, J.D., 1998. Adaptive optics Lorentzian point spread function. In: Bonaccini, D., Tyson, R.K. (Eds.), Adaptive Optical System Technologies. In: Proc. SPIE, vol. 3353. SPIE, Bellingham, WA, pp. 1030-1037.

Drummond, J.D., Fugate, R.Q., Christou, J.C., Hege, E.K., 1998. Full adaptive optics images of asteroids Ceres and Vesta: Rotational poles and triaxial ellipsoid dimensions. Icarus 132, 80-99.

Drummond, J.D., Christou, J., 2008. Triaxial ellipsoid dimensions and rotational poles of seven asteroids from Lick Observatory adaptive optics images, and of Ceres. Icarus 197, 480-496.

Li, J.-Y., McFadden, L.A., Thomas, P.C., Mutchler, M.J., Parker, J.Wm., Young, E.F., Russell, C.T., Sykes, M.V., Schmidt, B.E., 2010. Photometric mapping of Asteroid (4) Vesta's southern hemisphere with Hubble Space Telescope. Icarus 208, 238-251.

McCarthy, D.W., Freeman, J.D., Drummond, J.D., 1994. High resolution images of Vesta at 1.65 μm. Icarus 108, 285-297.

Minnaert, M., 1941. The reciprocity principle in lunar photometry. Astrophys. J. 93, 403-410.

Rayman, M.D., Fraschetti, T.C., Raymond, C.A., Russell, C.T. Dawn: A mission in development for exploration of main belt asteroids Vesta and Ceres. Acta Astronautica 58, 605-616.

Reddy, V., Gaffey, M.J., Kelley, M.S., Nathues, A., J.-Y., Li, Yarbrough, R., 2010. Compositional heterogeneity of Asteroid 4 Vesta's southern hemisphere: Implication for the Dawn Mission. Icarus, accepted.

Russell, C.T., and 15 colleagues, 2007. Dawn Mission to Vesta and Ceres. Earth Moon Planets 101, 65-91.

Seidelmann, P.K., and 14 colleagues, 2007. Report of the IAU/IAG working group on cartographic coordinates and rotational elements: 2006. Celestial Mechanics and Dynamical Astronomy 98, 155-180.

Thomas, P.C., Binzel, R.P., Gaffey, M.J., Zellner, B.H., Storrs, A.D., Wells, E., 1997a. Vesta: Spine pole, size, and shape from HST images. Icarus 128, 88-94.

Thomas, P.C., Binzel, R.P., Gaffey, M.J., Storrs, A.D., Wells, E.N., Zellner, B.H., 1997b. Impact excavation on Asteroid 4 Vesta: Hubble Space Telescope results. Science 277, 1492-1495.

Table 1. Summary of previously reported measurements of Vesta's pole orientation derived from limb-fitting.

Date	Phase angle (º)	Sub-Earth latitude* (º)	RA (º)	Dec (º)	Error (º)	Method**	References
Nov 16, 1983	12.5	+17	315	+41	3.8	SI	1
Oct 14, 1986	7.1	-13	274	+48	7.3	SI	2
Nov 30, 1990	7.5	+1	324	+44	2.2	SI IR	3
Feb 22, 1992	9.4	+18	300	+32	8.4	SI IR	3
Sep 20, 1993	12.0	-21	299	+35	6.9	AO	4
Nov 30, 1994	11.6	-21	299	+39	10	HST	5
Apr 27, 1996	8.3	-4	332	+42	1.5	AO	4
May 7, 1996	5.2	-3	308	+48	10	HST	5
May 11, 1996	5.2	-2	335	+45	0.8	AO	4
Oct 18, 1997	4.7	-8	275	+42	2.0	AO	6
Oct 20, 1997	4.8	-8	300	+45	0.7	HST	7
Aug 29, 2004	9.02	-18	321	+40	1.6	AO	7
Feb 11, 2006	15.8	+16	294	+8	7.5	AO	7

References:

1. Drummond et al. (1988)
2. Drummond and Hege (1989)
3. McCarthy et al. (1994)
4. Drummond et al. (1998)
5. Thomas et al. (1997a)
6. Drummond (1998)
7. Drummond and Christou (2008)

* Calculated with pole (301º, 41º).

** SI: speckle interferometry; IR: infrared; AO: adaptive optics

Table 2. Summary of all HST images used in our work.

Year	# of images	Camera	Filters	RA of Vesta (º)	Pixel scale (km/pix)	Phase angle (º)	Observer latitude* (º)	Solar latitude* (º)
1994	56	WFPC2	F439W, F673N, F953N, F1042M	99.4	53.9	11	+26	+20
1996	78	WFPC2		229.6	37.8	5.2	-9.3	-4.3
2007	96	WFPC2		251.7	38.1	9.5	-19	-11
2010	216	WFC3	F373N, F469N, F673N, F953N	152.5	39.9	5.3	+22	+25

* Calculated from Thomas et al. (1997a) pole solution.

Table 3. Summary of images used in control point solution with HST data

	Total	F373N	F439W/F469N*	F673N	F953N	F1042M
1994	6	-	4	2	0	0
1996	7	-	5	2	0	0
2007	17	-	9	3	2	3
2010	52	23	22	4	2	-
Total	82	23	40	11	4	3

*F439W for 1994, 1996, and 2007 data, F469N for 2010 data.

Table 4. Summary of measurement from feature tracking with HST images.

Data	Filters	Projected pole angle (east of north) (º)	Error (º)
1994	F439W, F673N	-26.1	6.9
1996	F439W, F673N	+47.0	1.8
2007	F439W, F673N	+40.3	2.5
2010	F373N, F469N	+21.5	8.4

Table 5

	Previous pole (301º, 41º)	New pole (307.5º, 43.1º)
Change	-	5.3º
Obliquity	27.2º	26.3º
Equinox (RA, Dec) *	(38.3º, 8.2º)	(49.0º, 12.1º)

* Sun-centered (RA, Dec) of Vesta at vernal equinox.

Figure captions

Fig 1 - Summary of previous measurements from 1994 and 1996 HST data (Thomas et al., 1997a). Open symbols are control point solutions; solid symbols limb-fitting solutions; squares are from 1994 data; hexagons from 1996 data. The cross marks the combined solution reported by Thomas et al. (1997a), which is weighted towards 1994 limb and 1996 control point solutions due to their smaller residuals. The open circle at (305.1º, 43.4º) is the solution derived from all Vesta images from HST in 1994, 1996, 2007, and 2010 using control points.

Fig 2 - The upper panel shows the RA and Dec of all historical ground and HST observations listed in Table 1. The lower panel shows the distribution of sub-Earth latitude for the same observations. The geometry is calculated with a pole at (301º, 41º). The observing geometries of these observations used to determine the pole of Vesta from limb-fitting almost uniformly distribute over the whole parameter space.

Fig 3 - The large diamond symbol is the combination of all previous pole solutions from limb-fitting techniques with the observations listed in Table 1 and showed in Fig. 2. The contour lines are 1, 2, and 3-σ error ellipses. The 1-σ uncertainties are 3.1º in RA and 1.2º in Dec. The tilt of the long-axis of the error ellipse from horizontal is 3.6º. The small diamond symbols are the solutions from individual observations, with the three observations from October 14, 1986, October 18, 1997, and February 11, 2006 outside of the plotting range.

Fig 4 - Pole solutions of Vesta from HST data listed in Table 2 using feature-tracking method. Solid arcs are the great circles derived from each observation. The shadowed area following each line is the error of each great circle. The star is the currently used solution, and the square is the combined solution of all four great circles. The two ellipses are the statistical 1-

σ and 3-σ error ellipses. The long and short axes of the 1-σ error ellipse are 6.8º and 1.5º, respectively, and the tilt of the long-axis is 14.6º from horizontal.

Fig 5 - Summary of the pole solutions of Vesta derived in our work. The symbols are: star – currently used solution (301º, 41º); diamond – combined solution (307.5º, 43.6º) from all previous ground/HST limb-fitting solutions; open circle – solution from control point stereogrammetry using all HST data (305.1º, 43.4º); square – solution from feature tracking (309.3º, 41.9º); cross-in-circle – final solution (307.8º, 42.9º) from the combination of all three solutions with different methods. The three ellipses in thin lines are the 1-σ error ellipses of the three solutions; the ellipse in thick line is the 1-σ error ellipse of the final solution. The 1-σ error of the final solution is 2.9º in RA and 1.1º in Dec. Due to the projection from spherical coordinates, the actual 1-σ region of the pole is 2.1º along RA direction.

Fig. 1

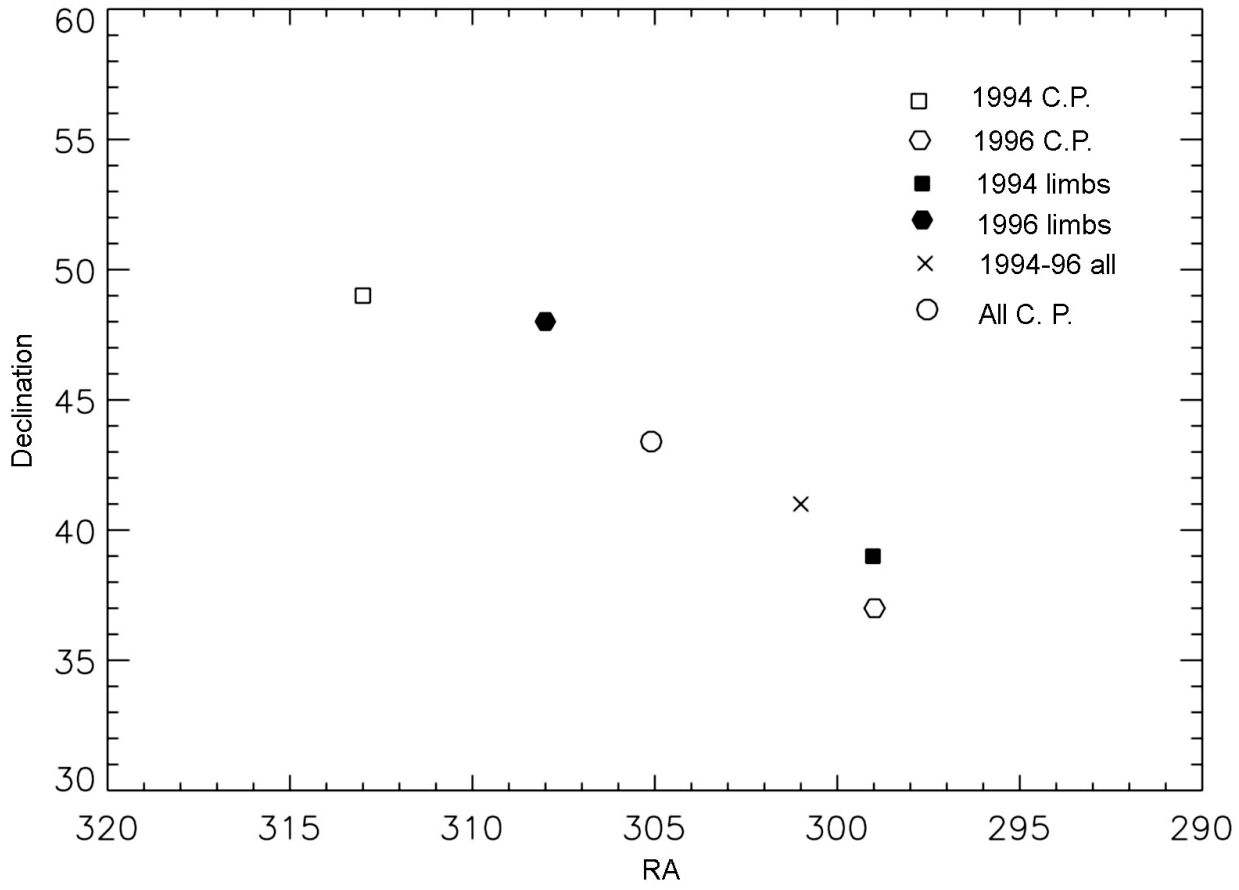
60
55
50
45
40
35
30
Declination
320
315
310
305
300
295
290
RA
1994 C.P.
1996 C.P.
1994 limbs
1996 limbs
1994-96 all
All C. P.

Fig. 2

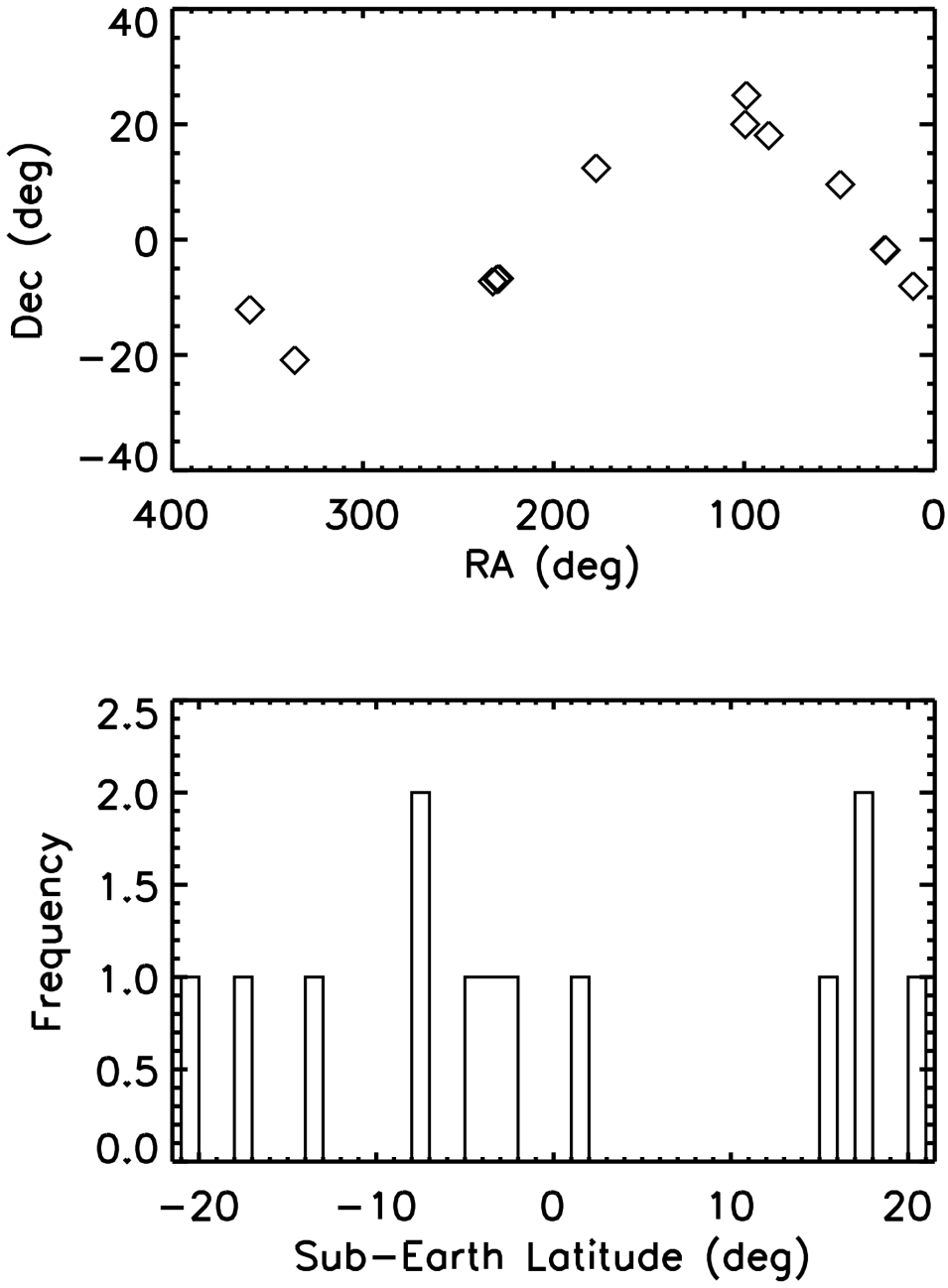
40
20
0
−20
−40
Dec (deg)
400
300
200
100
0
RA (deg)
2.5
2.0
1.5
1.0
0.5
0.0
Frequency
−20
−10
0
10
20
Sub−Earth Latitude (deg)

Fig. 3

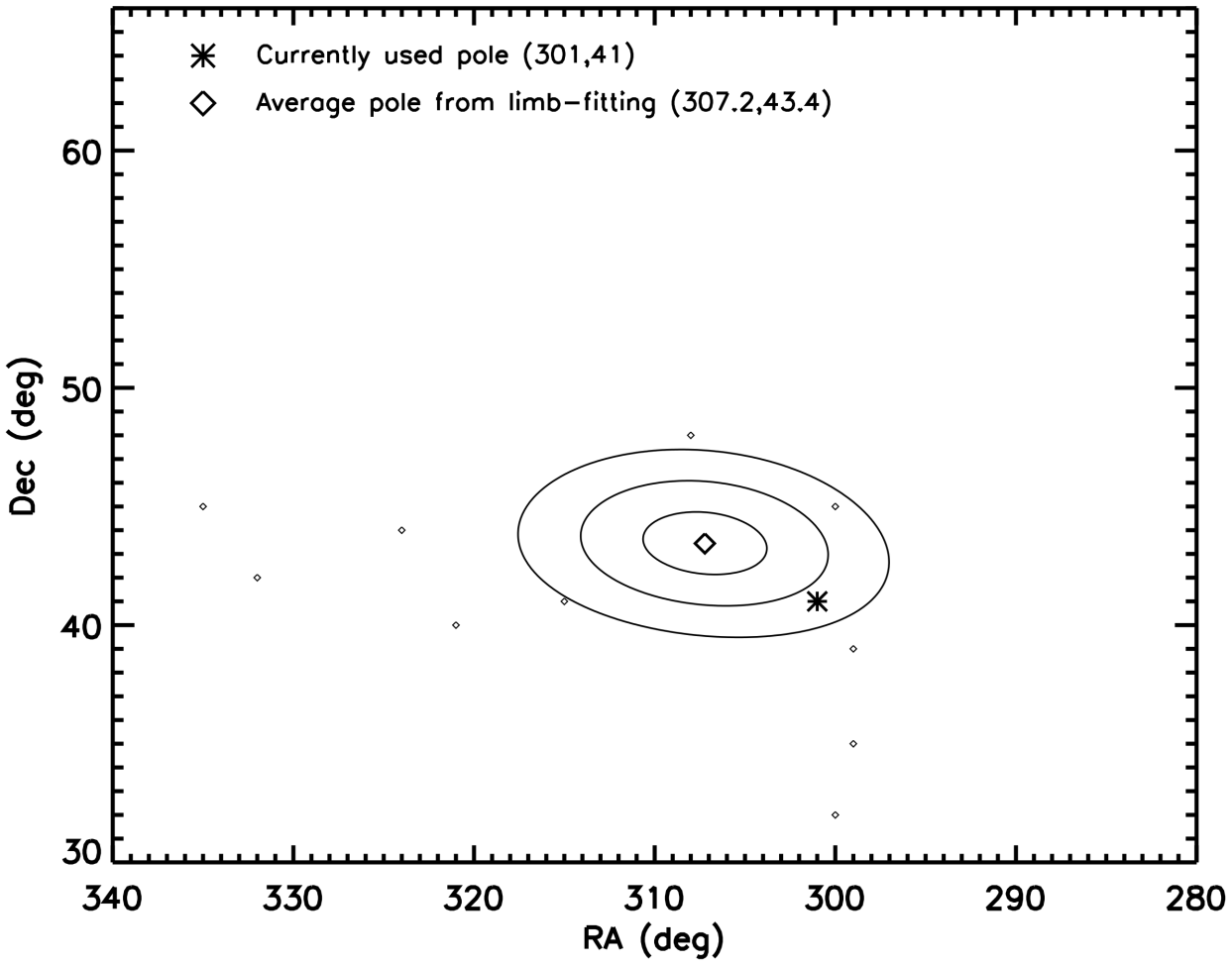
Currently used pole (301,41)
Average pole from limb−fitting (307.2,43.4)
60
50
40
30
Dec (deg)
340
330
320
310
300
290
280
RA (deg)

Fig. 4

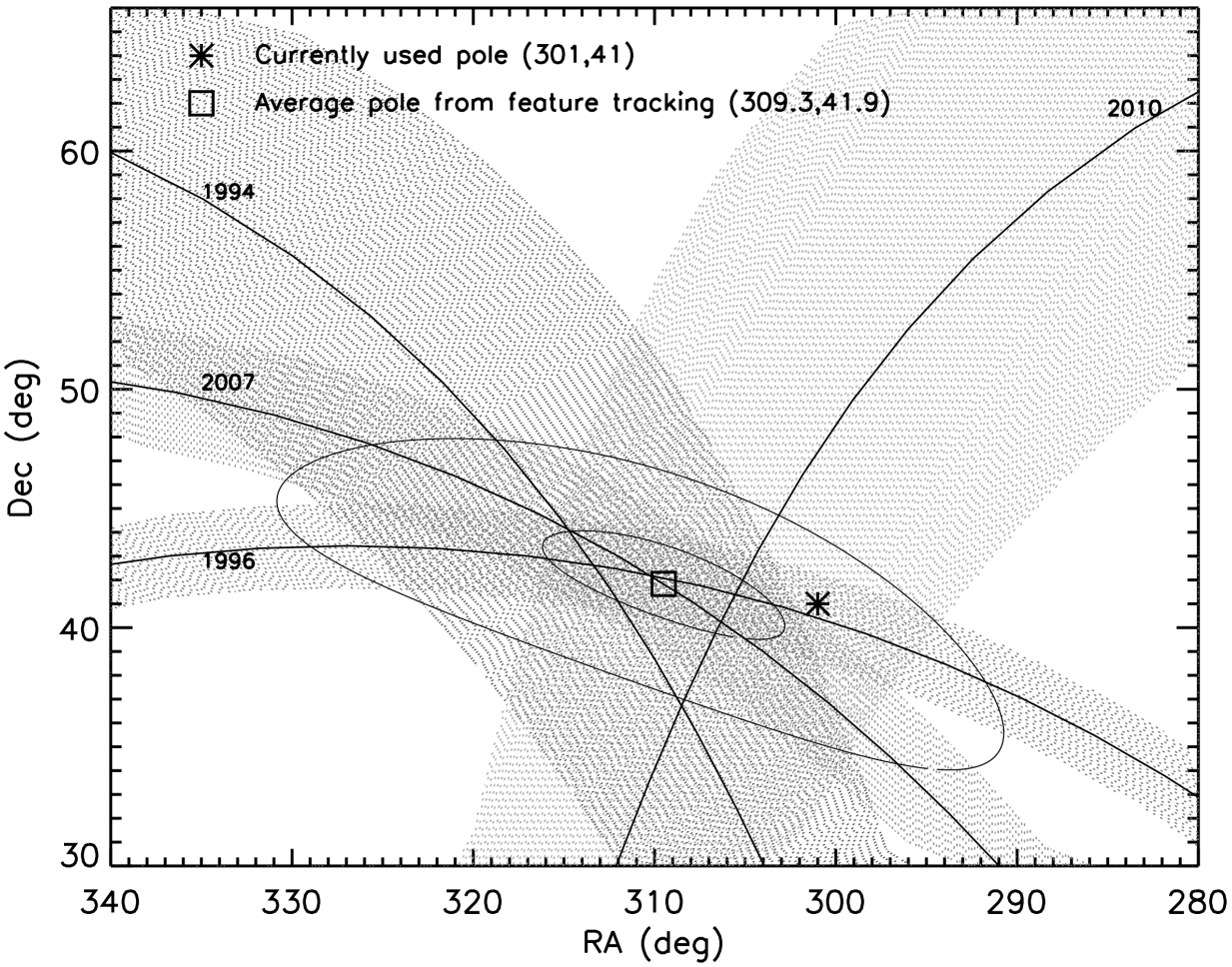
Currently used pole (301,41)
Average pole from feature tracking (309.3,41.9)
1994
2007
1996
2010
Dec (deg)
RA (deg)
60
50
40
30
340
330
320
310
300
290
280

Fig. 5